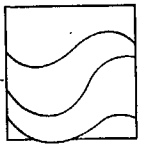

Enhanced rainfall in the mediterranean region during the last sapropel event

Mediterranean sea
Paleoclimatology
Paleoceanography
Sapropel events
Isotopes

Mer Méditerranée
Paléoclimatologie
Paléocéanographie
Evénement sapropèle
Isotope

Nejib KALLEL [a, b], Martine PATERNE [a], Jean-Claude DUPLESSY [a], Colette VERGNAUD-GRAZZINI [† c], Claude PUJOL [d], Laurent LABEYRIE [a], Maurice ARNOLD [a], Michel FONTUGNE [a] and Catherine PIERRE [c].
† *C. VERGNAUD-GRAZZINI died on May 1996.*

[a] Centre des Faibles Radioactivités, Laboratoire mixte CNRS-CEA, 91198 Gif-sur-Yvette cedex, France.

[b] Ecole Nationale d'Ingénieurs, B.P. "W" , 3038 Sfax, Tunisie.

[c] Laboratoire d'Océanographie Dynamique et de Climatologie, Université Pierre et Marie Curie, 4, place Jussieu, 75252 Paris cedex 05, France.

[d] Département de Géologie et Océanographie, CNRS, URA 197, Université de Bordeaux 1, 33405 Talence, France.

Received 05/01/96, in revised form 21/02/97, accepted 04/03/97.

ABSTRACT

Sea-surface temperature (SST) estimates for the last 10,000 years have been derived from foraminiferal fauna variations in ten cores from the Mediterranean Sea. For the eastern cores, modern analogs of fossil assemblages are found in the eastern Mediterranean Sea. In the Alboran and Tyrrhenian Seas, the best analogs originate from modern fauna located either in the western Mediterranean Sea or in the North Atlantic Ocean. During the last sapropel event, centred at about 8,000 years B.P., SSTs were similar to present in the eastern basin, whereas they were colder than today by about 1.5 °C in the Alboran Sea and 2.5 °C in the Tyrrhenian Sea.

Oxygen isotope measurements agree with ecological studies to show that *Globigerina bulloides* and *Globigerinoides ruber* alba grow their shell respectively in April-May and October-November. Assuming that these species deposited their shell in isotopic equilibrium with ambient water, we reconstructed Mediterranean surface water $\delta^{18}O$ and salinity during the last sapropel event (S_1). In contrast with the modern pattern in which evaporation dominates and salinity increases from west to east, the surface salinity during S_1 became almost homogeneous over the whole basin. This pattern suggests that the freshwater budget (precipitation plus runoff minus evaporation, P + R − E) was nearly equilibrated and that the Mediterranean Sea had ceased to be a concentration basin.

In the western Mediterranean Sea, the observed cooling can account for the formation of intermediate and deep waters with densities only slightly higher than that of the Atlantic subsurface water at the Gibraltar sill level. The Mediterranean outflow was then drastically reduced and the residence time of the Mediterranean deep water increased. In the eastern basin, no significant temperature change occurred during the Holocene. During the sapropel event S_1, surface salinities were not significantly different from those of the western basin and deep water colder and denser than those of the western basin could not form. At the level of the Siculo-Tunisian Strait, the cold western intermediate water penetrated

the deep eastern Mediterranean Sea. As a consequence, a permanent pycnocline was established between surficial and intermediate waters, preventing winter overturning and the supply of dissolved oxygen in the deeper part of the basin. This hydrological structure was responsible for the establishment of anoxia and the preservation of organic matter at the bottom in the eastern Mediterranean Sea.

RÉSUMÉ

Augmentation des pluies sur la région méditerranéenne pendant l'événement du dernier sapropèle.

Les variations de la température des eaux de surface en Méditerranée au cours de l'Holocène ont été estimées à partir des changements de la faune des foraminifères planctoniques à l'aide de la technique des analogues actuels. Dix carottes réparties dans les principaux bassins de cette mer montrent qu'à l'époque de la formation du dernier sapropèle (S_1) en Méditerranée orientale, il y a environ 8 000 ans, les températures de surface étaient environ 1,5 à 2,5 °C plus froides qu'aujourd'hui dans le bassin occidental alors qu'en Méditerranée orientale, elles étaient sensiblement égales à celles observées actuellement. Nous avons démontré, par l'analyse de sommets de carottes représentant les conditions actuelles, que les paléotempératures isotopiques obtenues à partir des foraminifères planctoniques *Globigerina bulloides* et *Globigerinoides ruber* alba sont linéairement liées aux températures de surface d'avril-mai et d'octobre-novembre respectivement.

Nous avons ensuite mesuré la composition isotopique de l'oxygène ($\delta^{18}O$) de *G. bulloides* et *G. ruber* pendant le maximum du dernier sapropèle et en avons déduit une estimation de la salinité des eaux de surface de la Méditerranée. Les résultats montrent que les salinités de surface de l'ensemble de la Méditerranée étaient sensiblement égales à celle à Gibraltar. Les apports d'eau douce compensaient donc les pertes par évaporation et la Méditerranée ne fonctionnait pas comme un bassin de concentration.

Dans le bassin occidental, le refroidissement observé permettait la formation d'eau intermédiaire et profonde avec des densités légèrement supérieures à celles des eaux de subsurface de l'Océan Atlantique Nord à la profondeur du seuil de Gibraltar. Ce faible gradient de densité au travers du détroit ne permettait qu'un échange réduit avec l'océan Atlantique, provoquant une augmentation du temps de résidence des eaux profondes en Méditerranée. Dans le bassin oriental, la salinité des eaux de surface était voisine de celle du bassin occidental. Des eaux profondes plus froides et plus denses que celles présentes à l'Ouest du détroit siculo-tunisien ne pouvaient se former. La circulation était donc inversée entre les deux bassins et le fond de la Méditerranée Orientale était occupé par les eaux intermédiaires du bassin occidental. Par conséquent, une pycnocline permanente s'était développée entre les eaux de surface et les eaux profondes. La convection et l'oxygénation des eaux profondes étaient bloquées dans le bassin oriental, favorisant l'établissement des conditions anoxiques responsables de la disparition de la vie benthique et de la préservation de la matière organique sur le fond.

Oceanologica Acta, 1997, **20**, 5, 697-712.

INTRODUCTION

The Mediterranean Sea, which is connected to the Atlantic Ocean through the Gibraltar Strait, is limited to the south by the Sahara which is under the influence of subtropical highs and to the north by the European-Asian temperate-to-subtropical region. During the Quaternary, all these continental areas experienced drastic climatic changes affecting both the temperature regime and the hydrology (Petit-Maire *et al.*, 1991; Bottema, 1991; Fontes and Gasse, 1991). The response of the Mediterranean Sea to these changes is still poorly documented. In particular, organic-rich horizons inserted in the normal marl oozes of the basin are one of the main features characterizing the Holocene and Pliocene-Pleistocene sediments of the eastern Mediterranean Sea. These centimetric layers, called sapropels, comprise black sediments containing abundant, well-preserved planktonic microfossils, but often devoid

of benthic fossils (Williams *et al.*, 1978). Their origin has been extensively debated, and three hypotheses have received the greatest attention: i) an increase of biological productivity, which would increase oxygen utilization in the water column and hence preservation of organic matter on the bottom (Berger, 1976; Sutherland *et al.*, 1984; Schrader and Matherne 1981; Calvert, 1983; Rohling and Gieskes, 1989; Rohling, 1991; Calvert *et al.*, 1992; Sarmiento *et al.*, 1988; Thunell and Williams, 1989; Rohling, 1994); ii) an increased preservation of deposited organic matter by bottom water anoxia resulting from the stratification of the whole water column, as a consequence of a low salinity surface layer that would prevent winter overturning and renewal of deep water oxygen (Bradley, 1938; Huang and Stanley, 1972; Cita *et al.*, 1977; Ryan and Cita, 1977; Williams *et al.*, 1978; Rossignol-Strick *et al.*, 1982; Thunell *et al.*, 1984; Vergnaud-Grazzini *et al.*, 1977, 1986) ; iii) finally, Howell and Thunell (1992) suggested that sapropels resulted from some combination of both enhanced productivity and water column stratification.

The last sapropel event (S_1), extensively dated by the Accelerator Mass Spectrometry (AMS) ^{14}C method, was found to be centred at around 8,000 years B.P. (Troelstra *et al.*, 1991; Fontugne *et al.*, 1994). It coincides with a negative peak in the planktonic foraminiferal $\delta^{18}O$ record (Williams *et al.*, 1978). This peak may be explained either by a SST increase or a salinity decrease. We developed a micropaleontologic transfer function which allows us to estimate SST from foraminiferal fauna changes, using the modern analog technique (Hutson, 1979; Prell, 1985). We then estimated Holocene SST variations in ten deep sea cores raised from the main basins of the Mediterranean Sea. Finally, sea-surface salinity changes were calculated from the $\delta^{18}O$ variations of two common planktonic foraminiferal species, *Globigerina bulloides* and *Globigerinoides ruber* alba, whose $\delta^{18}O$ values were calibrated using an extensive core-top data set representative of modern conditions.

PAST SEA-SURFACE TEMPERATURE ESTIMATES

Modern Analog Technique

In the Mediterranean Sea, SSTs have been previously estimated for the Last Glacial Maximum (about 18,000 years B.P.), by comparing the glacial faunas to those of surface Atlantic sediment (Thiede, 1978; Thunell, 1979). However, no SST estimates were derived for the last 10,000 years, because the Holocene faunas are different from those of the Atlantic Ocean. To overcome this difficulty, we developed a comprehensive reference modern data base containing planktonic foraminiferal counts from both 128 core tops from the Mediterranean Sea and 123 core tops from the North Atlantic Ocean (Fig. 1). The mean monthly temperature at the location of each core was taken from Levitus (1982).

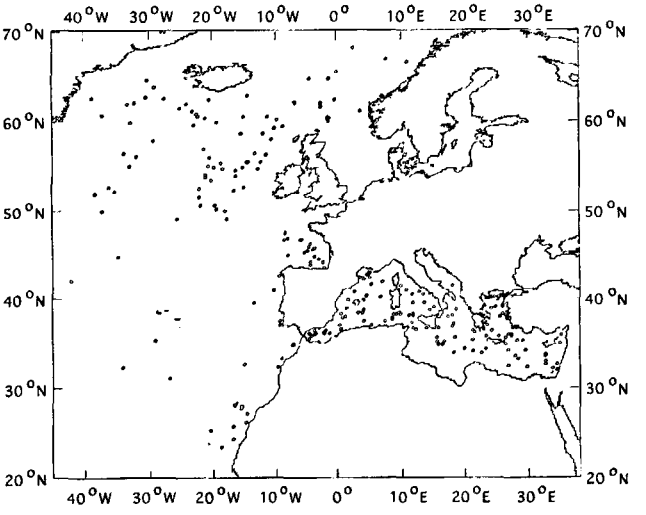

Figure 1

Core top location of the micropaleontological reference data base.

We first assessed the quality of this data base for generating SST estimates. For each modern core top sample, we identified the ten most similar samples in the reference data base (excluding the analysed core top itself) using the squared chord distance dissimilarity coefficient (Prell, 1985). Following the Modern Analog Technique (MAT) developed by Hutson (1979), we estimated SSTs during the most productive periods (April-May and October-November) at the core location by computing the average of the April-May and October-November SSTs at the location of the ten selected cores. The temperature estimates are highly correlated with the Levitus data (Table 1; Fig. 2). The slope of the regression line between estimated and observed SSTs is not significantly different from 1; the mean difference between observed and estimated SSTs is less than 0.1 °C with a standard deviation < 1 °C.

Table 1

Summary of the fit between observed (Levitus) and estimated (by the modern analog technique) April-May and October-November SSTs for the Mediterranean core top foraminiferal counts of the reference data base. For each case, the following statistics are given: r^2 = the correlation coefficient between observed and estimated SST; $\overline{\Delta T}$ = the mean SST residual (estimated - observed) and $\sigma\overline{\Delta T}$ = the standard deviation of the residuals ($\overline{\Delta T}$).

	Correlation coefficient (r^2)	$\overline{\Delta T}$ (°C)	$\sigma\overline{\Delta T}$ (°C)
April-May	0.750	0.086	0.617
October-November	0.754	0.022	0.965

Isotopic calibration of *Globigerina bulloides* and *Globigerinoides ruber*

Two planktonic foraminiferal species are generally abundant in Mediterranean Sea cores: *G. bulloides* dominates in the western basin, whereas *G. ruber* dominates in the eastern basin. We measured the $\delta^{18}O$ value of both species (Tables 2, 3), which depends on both

Table 2

Summary of the data used for the calibration of the oxygen isotopic ratio of G. bulloides. G. bulloides $\delta^{18}O$ *values from 34 Mediterranean core tops; Modern sea-surface salinity from Levitus Atlas (1982); Sea surface* $\delta^{18}O$*, calculated from salinity, using the Mediterranean surface water* $\delta^{18}O$*/Salinity relationships (Fig. 3); Levitus Mean (April-May) SST; Isotopic temperature calculated from* G. bulloides $\delta^{18}O$ *using Shackleton relationship (1974).*

Core	Latitude	Longitude	$\delta^{18}O$ *G. bulloïdes*	Modern sea surface salinity	Calculated sea surface $\delta^{18}O$ vs. SMOW	April-May sea surface temperature	Isotopic temperature	Data source
KS82-30	26°27'N	03°53'W	0.65	36.65	0.85	16.38	16.6	1
SU81-07	35°57'N	03°48W	0.81	36.59	0.82	16.51	15.8	Gif
SU92-33	38°25'N	00°34'E	0.63	37.26	1.09	16.40	17.8	Gif
SU81-03	37°58'N	00°50'E	0.88	37.13	1.04	16.78	16.4	Gif
MD90-901	39°57'N	01°35'E	1.02	37.38	1.15	16.11	16.3	Gif
70-KS-06	38°31'N	04°00'E	0.50	37.07	1.02	16.63	18.0	2
Ecor1Ki05	42°47'N	04°39'E	1.09	37.51	1.20	14.59	16.2	Gif
Ecor4Ki50	42°50'N	04°49'E	1.89	37.51	1.20	14.59	12.8	Gif
A1A6	42°50'N	04°50'E	1.36	37.51	1.20	14.59	15.0	Gif
A1A2	42°50'N	04°50'E	1.34	37.51	1.20	14.59	15.1	Gif
A1A5	42°50'N	04°50'E	1.24	37.51	1.20	14.59	15.5	Gif
B1A6	42°50'N	04°50'E	1.16	37.51	1.20	14.59	15.9	Gif
Ecor1Ki15	42°24'N	04°57'E	1.12	37.51	1.20	14.59	16.1	Gif
Ecor2Ki25	42°56'N	05°06'E	1.19	37.79	1.31	14.86	16.3	Gif
KET80-22	40°35'N	11°43'E	1.21	37.89	1.35	16.11	16.4	Gif
AC85-4	41°45'N	11°46'E	1.30	37.93	1.37	15.79	16.0	3
KET80-40	36°47'N	11°49'E	1.00	37.24	1.09	16.01	16.1	Gif
CS72-37	36°41'N	12°17'E	1.31	37.32	1.12	16.09	14.9	Gif
70-CS-05	35°44'N	13°11'E	0.77	37.55	1.21	16.95	17.7	4
KET80-19	40°33'N	13°21'E	1.54	37.92	1.37	16.25	15.0	Gif
KET80-04	39°40'N	13°34'E	1.02	37.86	1.34	16.33	17.1	Gif
DED87-07	39°41'N	13°34'E	0.97	37.86	1.34	16.33	17.4	Gif
KET80-03	38°49'N	14°30'E	1.00	38.09	1.46	16.42	17.7	Gif
IN68-21	42°53'N	14°47'E	0.95	37.83	1.33	15.76	17.4	5
KET80-11	39°10'N	15°05'E	0.95	38.14	1.47	16.20	18.0	Gif
KET80-68	38°06'N	17°18'E	0.93	38.30	1.50	16.98	18.2	Gif
MD90-916	41°31'N	17°58'E	1.05	37.73	1.29	16.44	16.8	Gif
KET82-16	41°31'N	17°59'E	1.42	37.73	1.29	16.44	15.2	Gif
RC9-191	38°11'N	18°02'E	1.19	38.38	1.52	17.44	17.2	Gif
80-KB-11	36°30'N	24°20'E	1.43	38.79	1.60	17.30	16.5	Gif
TR171-27	33°50'N	25°59'E	1.10	38.91	1.62	18.04	18.0	6
V10-49	36°05'N	26°50'E	0.79	39.07	1.65	17.58	19.5	Gif
V10-51	35°55'N	27°18'E	0.88	39.13	1.67	18.19	19.2	Gif
TR172-22	35°19'N	29°01'E	1.20	39.08	1.66	18.33	17.7	6

1- Pujol and Vergnaud-Grazzini, 1989; 2- Vergnaud-Grazzini *et al.*, 1986; 3- Capotondi *et al.*, 1989; 4- Vergnaud-Grazzini *et al.*, 1988; 5- Jorissen *et al.*, 1993; 6- Thunell *et al.*, 1977.

SST and sea water $\delta^{18}O$ at the time of shell formation (Epstein *et al.*, 1953; Shackleton, 1974).

A first attempt to estimate the modern Mediterranean sea water $\delta^{18}O$ (δw) from salinity measurements was made by Thunell *et al.* (1987) using the simple relationship:

δw (‰) = 0.41*Salinity – 14.34

However, this relationship was derived from a small number of measurements. In order to improve the relationship linking Mediterranean surface water $\delta^{18}O$ to salinity, we used a new extensive data base of surface water samples (between 0 and 100 m) comprising both Atlantic and Mediterranean samples. Thirty-four water samples were collected from the tropical eastern Atlantic Ocean, close to Gibraltar and are characteristic of the water penetrating the Mediterranean Sea through the Gibraltar Strait (Pierre *et al.*, 1994). One hundred and seven samples and 75 samples were collected in the western and eastern Mediterranean Sea respectively. The complete hydrological profiles will be discussed elsewhere (Pierre, in press). We only discuss the relationship between the salinity and the surface water $\delta^{18}O$. The data show a broad band in which $\delta^{18}O$ generally increases with salinity, in accordance with the preferential evaporation of the light molecule $H_2{}^{16}O$. As demonstrated by Craig and Gordon (1965), the deviation from a simple linear correlation is due to the differing $^{18}O/^{16}O$ ratio in precipitation in the different basins and the kinetic effects at the sea surface during evaporation of sea water. For samples from the whole Mediterranean Sea, the relationship linking modern surface water $\delta^{18}O$ to salinity is:

$\delta^{18}O$ = 0.25 S-8.23 (r = 0.884) (Pierre, in press)

However, we show below that during sapropel 1 deposition, the Mediterranean Sea surface water $\delta^{18}O$ values were significantly lower than today. This indicates that Atlantic

Table 3

Summary of the data used for the calibration of the oxygen isotopic ratio of G. ruber. G. ruber $\delta^{18}O$ *values from 40 Mediterranean core tops; Modern sea-surface salinity from Levitus Atlas (1982); Sea surface* $\delta^{18}O$*, calculated from salinity, using the Mediterranean surface water* $\delta^{18}O$*/Salinity relationships (Fig. 3); Levitus Mean (October-November) SST; Isotopic temperature calculated from* G. ruber $\delta^{18}O$.

Core	Latitude	Longitude	$\delta^{18}O$ *G. ruber*	Modern sea surface salinity	Calculated sea surface $\delta^{18}O$ vs. SMOW	Oct.-Nov. sea surface temperature	Isotopic temperature	Data source
KS82-30	36°27'N	03°53'W	0.07	36.75	0.89	18.94	19.3	1
KS82-31	36°09'N	03°16'W	0.27	36.75	0.89	18.94	18.4	1
SU92-33	38°25'N	00°34'E	0.05	37.40	1.15	20.30	20.6	Gif
SU81-03	37°58'N	00°50'E	0.07	37.21	1.08	20.26	20.2	Gif
MD90-901	39°57'N	01°35'E	0.56	37.51	1.20	19.70	18.5	Gif
70KS06	38°31'N	04°00'E	0.40	37.35	1.14	20.25	19.0	2
Ecor1Ki05	42°47'N	04°39'E	1.01	38.06	1.45	18.14	17.7	Gif
Ecor2Ki35	42°46'N	04°48'E	0.80	38.06	1.45	18.14	18.6	Gif
KET80-22	40°35'N	11°42'E	0.37	38.00	1.40	19.97	20.3	Gif
KET80-40	36°47'N	11°49'E	−0.14	37.48	1.19	20.69	21.6	Gif
CS72-37	36°41'N	12°17'E	0.22	37.56	1.22	20.84	20.1	Gif
KET80-19	40°33'N	13°21'E	0.71	37.98	1.39	20.21	18.7	Gif
KET80-04	39°40'N	13°34'E	0.51	37.93	1.37	20.36	19.5	Gif
DED87-07	39°41'N	13°35'E	0.51	37.93	1.37	20.36	19.5	Gif
KET80-03	38°49'N	14°30'E	0.54	38.09	1.46	20.56	19.8	Gif
KET80-11	39°10'N	15°05'E	0.50	38.06	1.45	20.19	19.9	Gif
KET80-68	38°06'N	17°18'E	0.36	38.29	1.50	20.06	20.8	Gif
MD84-658	35°02'N	17°38'E	0.58	38.33	1.51	21.54	19.8	Gif
MD90-916	41°30'N	17°58'E	0.74	37.85	1.34	17.78	18.4	Gif
KET82-16	41°31'N	17°59'E	0.79	37.85	1.34	17.78	18.1	Gif
RC9-191	38°11'N	18°02'E	0.59	38.43	1.53	20.04	19.9	Gif
V10-67	35°42'N	20°43'E	0.60	38.69	1.58	21.53	20.1	7
RC9-183	34°30'N	23°25'E	0.52	38.91	1.62	21.53	20.6	Gif
80KB11	36°30'N	24°20'E	0.89	38.78	1.60	20.48	18.9	Gif
MD84-656	33°23'N	24°46'E	0.61	38.99	1.64	21.95	20.3	Gif
RC9-181	33°25'N	25°00'E	0.30	39.06	1.65	22.01	21.8	8
RC9-180	34°05'N	25°24'E	0.77	39.07	1.66	21.54	19.6	Gif
TR171-27	33°50'N	25°59'E	0.45	39.06	1.65	22.01	21.1	6
81-MC-08	35°47'N	26°36'E	0.44	39.10	1.66	20.97	21.2	Gif
V10-49	36°05'N	26°50'E	0.58	38.99	1.64	20.14	20.4	Gif
82KS-01	34°22'N	27°09'E	0.24	39.19	1.68	21.81	22.2	2
80KB28	34°51'N	27°15'E	0.88	39.19	1.68	21.81	19.2	9
V10-51	35°55'N	27°18'E	0.52	39.19	1.68	21.16	20.9	Gif
RC9-178	33°44'N	27°55'E	0.12	39.15	1.67	22.34	22.7	Gif
MD90-220	35°18'N	28°13'E	0.32	39.28	1.70	21.55	21.9	Gif
TR172-22	35°19'N	20°01'E	0.55	39.29	1.70	22.13	20.8	6
P6508-36	32°44'B	30°31'E	0.37	39.12	1.66	23.79	21.5	10
Core 17	35°30'N	33°20'E	−0.60	39.25	1.69	23.40	26.2	11
Core 190	36°00'N	33°23'E	−0.25	39.25	1.69	23.40	24.5	11
MD84-629	32°04'N	34°21'E	−0.30	39.16	1.67	24.56	24.7	Gif

1- Pujol and Vergnaud-Grazzini, 1989; 2- Vergnaud-Grazzini *et al.*, 1986; 3- Capotondi *et al.*, 1989; 4- Vergnaud-Grazzini *et al.*, 1988; 5- Jorissen *et al.*, 1993; 6- Thunell *et al.*, 1977; 7- Vergnaud-Grazzini, 1975; 8- Vergnaud-Grazzini *et al.*, 1977; 9- Vergnaud-Grazzini *et al.*, 1989; 10- Jenkins and Williams, 1984; 11- Buckley *et al.*, 1982.

waters entering at Gibraltar were much less evaporated than today during their circulation in both eastern and western mediterranean basins. In order to generate a $\delta^{18}O$/salinity relationship which would be valid for the whole Holocene, we added the tropical eastern Atlantic measurements to those from the Mediterranean Sea. We then distinguished in Figure 3 two domains in which the relationship between $\delta^{18}O$ and salinity is approximately linear:

• for salinities lower than 38:

$\delta w = 0.41*Salinity - 14.18 \qquad r = 0.92$

This relationship is close to that used by Thunell *et al.* (1987) and is valid for the eastern Atlantic near Gibraltar and the southern part of the western Mediterranean Sea.

• in those regions where evaporation has a strong imprint on the surface salinity (the eastern and the northern western Mediterranean Sea), a lower slope is observed. We calculated for salinities larger than 37.5 the empirical relationship:

$\delta w = 0.199*Salinity - 6.12 \qquad r = 0.63$

The δw values calculated by both relationships are very close for salinity values in the range 37.5-38. We therefore used the first relationship to estimate the Mediterranean surface water $\delta^{18}O$ for salinity lower than 38 and the second relationship for salinity higher than 38. For a given salinity, the standard deviation for each δw estimate is 0.14 ‰. The $\delta^{18}O$ estimates calculated by this method

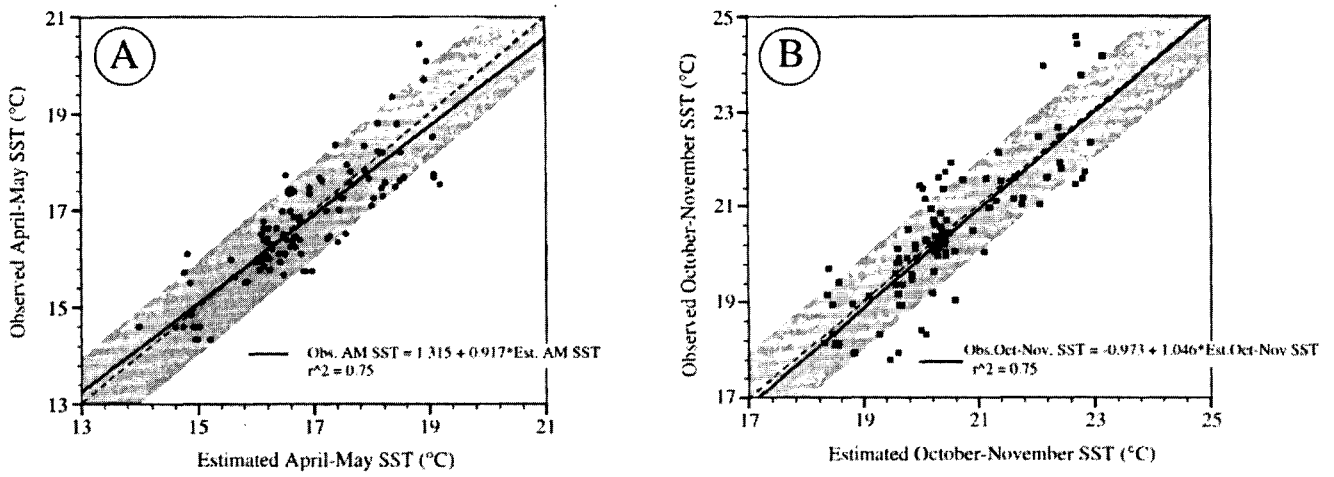

Figure 2

Comparison of observed (Levitus data) and estimated (by the modern analog technique) SSTs on the Mediterranean core top foraminiferal counts of the reference data base: A, for April-May and B, for October- November.

or using the relationship of Pierre (in press) are similar within the standard deviation of both methods for modern mediterranean Sea samples.

Foraminiferal isotopic temperatures have then been calculated using the palaeotemperature equation of Shackleton (1974). The standard error associated with that on the estimation of the sea water $\delta^{18}O$ is 0.7 °C. Following the approach introduced by Duplessy *et al.* (1991), the isotopic temperatures were compared with those prevailing during the annual cycle (Levitus, 1982). A statistical analysis shows that the best linear fit is obtained between the isotopic temperature of *G. bulloides* and the April-May Levitus SST, with a correlation coefficient r = 0.69 significant at the 99% confidence level (Fig. 4*a*). The slope

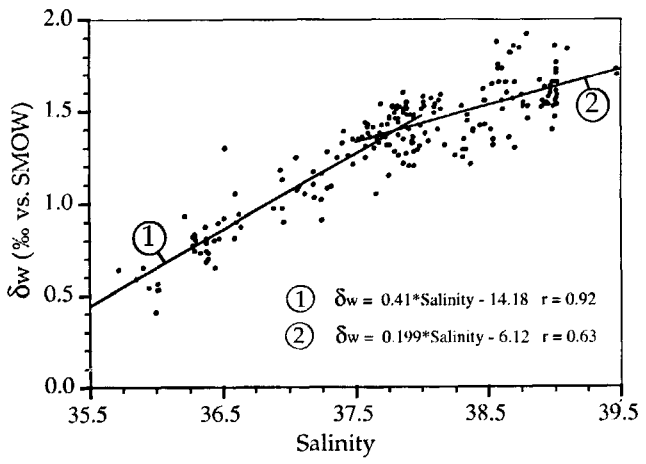

Figure 3

Plot of the $\delta^{18}O$ value against salinity for water samples collected in the upper 100 m from the tropical eastern Atlantic Ocean, close to Gibraltar (34 water samples) and from the western (107 samples) and eastern Mediterranean Seas (75 samples). The Atlantic data are from Pierre et al., (1994) and the Mediterranean data from Duplessy (1972), Duplessy and Fieux (1972), Stahl and Rinow (1973) and Pierre et al., (1986; in press).

of the regression line is 0.87 ± 0.16 and the best fit estimate differs by less than 0.7 °C from the simple relationship: $T_{isotope}$ = Mean (April-May) SST. The mean difference between the isotopic temperature estimate and Mean (April-May) SST is 0.4 °C with a standard deviation of 1 °C. The isotopic temperature of *G. ruber* is significantly correlated with October-November SST (r = 0.81), and the slope of the regression line is 0.94 ± 0.11 (Fig. 4*b*). This best fit estimate differs by less than 0.6 °C from the October-November SST. The mean difference between the isotopic temperature estimate and Mean (October-November) SST is close to –0.4 °C with a standard deviation of 1.1 °C.

The correlation of the isotopic temperature with SST for other months is significantly weaker than the best estimates derived above. We therefore consider these relationships as calibrations for *G. bulloides* and *G. ruber* and assume simply that the isotopic temperatures of these species reflect respectively the mean April-May and October-November SSTs. These results are in agreement with the present annual production cycle. Two seasonal peaks of productivity are observed, the first from late winter to early spring and the second during late summer and autumn. The *G. bulloides* bloom is restricted to spring, whereas *G. ruber* grows mainly during autumn (Vergnaud-Grazzini *et al.*, 1989; Pujol and Vergnaud-Grazzini, 1989, 1995).

We have then compared the oxygen isotope fractionation ($\delta^{18}O_{foraminifera}$ - δw) of both these species with their growth temperature (Fig. 4*c*). The regression line has a high correlation coefficient (r = 0.91), and a slope close to that predicted by isotopic equilibrium (Shackleton, 1974).

Estimates of SST during the last sapropel event

Planktonic foraminiferal counts were performed in ten cores located in the major Mediterranean Sea basins (Fig. 5*a*). We used the MAT to compare fossil planktonic foraminiferal samples to the reference data base and to identify, for each fossil association, the best modern

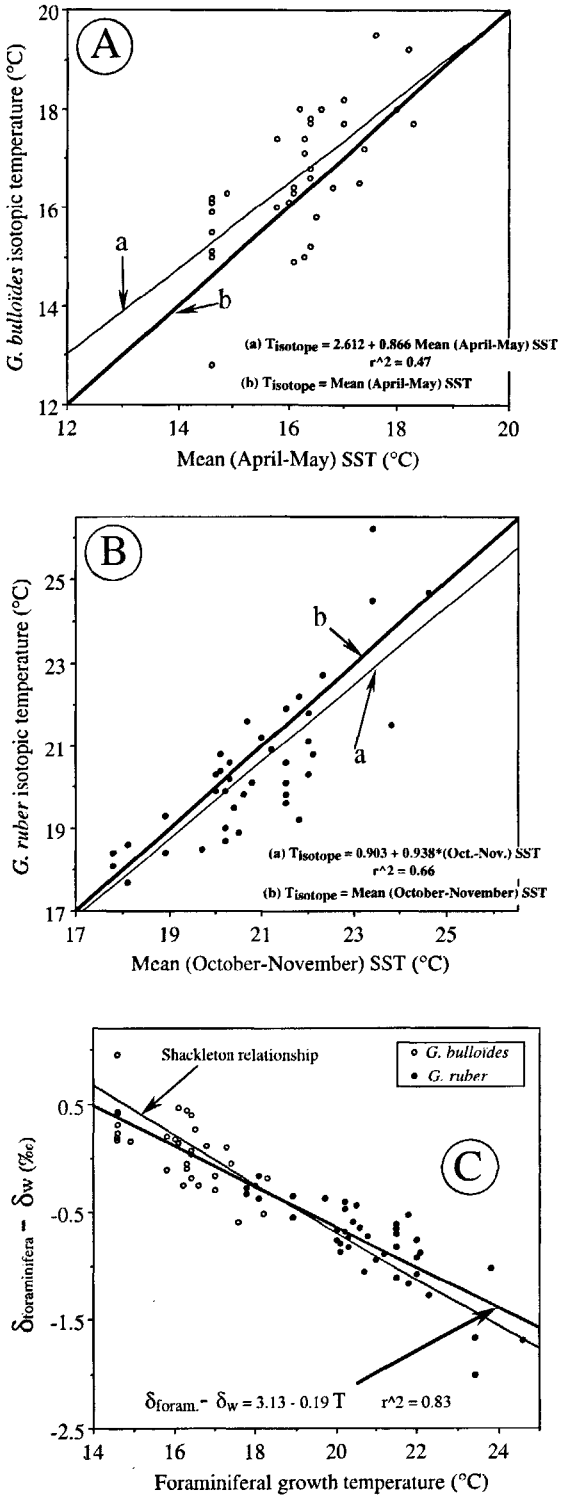

Figure 4

A: Plot of the isotopic temperature calculated from G. bulloides $\delta^{18}O$ values against Levitus mean sea surface temperature (SST) during April to May for 34 Mediterranean core tops. We have also compared the regression line obtained from these data (a) with the simple relationship (b) : Tisotope = Mean (April-May) SST.

B: Plot of the isotopic temperature calculated from G. ruber $\delta^{18}O$ values against Levitus mean SST during October to November for 40 Mediterranean core tops. We have also compared the regression line obtained from these data (a) with the simple relationship (b): Tisotope = Mean (October-November) SST.

C: Plot of oxygen isotope fractionation ($\delta^{18}O$ foraminifera-δw) of G. bulloides *and* G. ruber *from the tops (modern conditions) of 47 Mediterranean deep sea cores with their seasonal growth temperature. The Shackleton relationship (1974) between oxygen isotope fractionation ($\delta^{18}O$ foraminifera – $\delta^{18}w$) and temperature is also shown.*

analogs. Following Overpeck *et al.* (1985), we assumed that dissimilarity coefficients lower than 0.2 are indicative of good modern analogs. During the Holocene, good modern analogs of fossil samples were generally found in the Mediterranean Sea. However, the best analogs of fossil fauna during S_1 come from the North Atlantic Ocean in the Alboran Sea and the Tyrrhenian Sea.

In the Tyrrhenian Sea, a poorly marked black sediment layer coincides with a negative peak in the $\delta^{18}O$ record. This peak also coincides with a rhyolitic tephra-layer of the same age as S_1, observed both in the Tyrrhenian and Adriatic sea sediment cores (Paterne *et al.*, 1988; Fontugne *et al.*, 1989). These correlations show that the negative $\delta^{18}O$ peak in the Alboran Sea record was synchronous with the sapropel S_1 of the eastern Mediterranean Sea.

Holocene SST records are reported in Figures 5*a*, 5*b*. During S_1, April-May and October-November SSTs are colder than today by about 2.5 °C in the Tyrrhenian Sea and 1.5 °C in the Alboran Sea. During that period, the Tyrrhenian Sea fauna was dominated (≈ 60%) by *Neogloboquadrina pachyderma* (right coiling) and the fossil planktonic foraminiferal assemblage is very similar to that observed in the modern Gulf of Gascogne. *N. pachyderma* (right coiling) is most prolific today in waters warmer than 7 °C and colder than 12 °C (Bé and Tolderlund, 1971). In the modern Mediterranean Sea, it is dominant in the Gulf of Lions where winter SSTs are close to 13 °C (Pujol and Vergnaud-Grazzini, 1995). In the Alboran Sea, the two coiling forms of *N. pachyderma* show a significant increase at the time of S_1. The right-coiling form exceeded 30% of the foraminiferal fauna (whereas it is only about 8% under modern conditions) and the percentage of left-coiling one was of about 3%. This increase is responsible for the cold SSTs provided by the transfer function.

By contrast, the eastern Mediterranean SSTs were not significantly different from the modern values. These results show that the negative $\delta^{18}O$ peak in the planktonic foraminiferal records in the eastern Mediterranean Sea is not explained by a warming, but rather reflects a surface water $\delta^{18}O$ and salinity decrease, as previously suggested (Huang and Stanley, 1972; Cita *et al.*, 1977; Ryan and Cita, 1977; Williams *et al.*, 1978; Rossignol-Strick *et al.*, 1982; Thunell *et al.*, 1984).

MEDITERRANEAN SURFACE SALINITY PATTERN ASSOCIATED WITH THE LAST SAPROPEL

In this section, we tentatively quantify the surface water $\delta^{18}O$ and salinity changes in the Mediterranean Sea during the last sapropel event. Surface water $\delta^{18}O$ estimates were obtained on 47 deep sea cores (Table 4; Fig. 6*a*), by solving the palaeotemperature equation (Shackleton, 1974) and assuming that the planktonic foraminifera deposited their shells in isotopic equilibrium with the growth temperature as defined for modern conditions. We assumed that SSTs were similar to the present in the eastern basin, and lower than today by 1.5 °C in the Alboran Sea and 2.5 °C in the Tyrrhenian Sea.

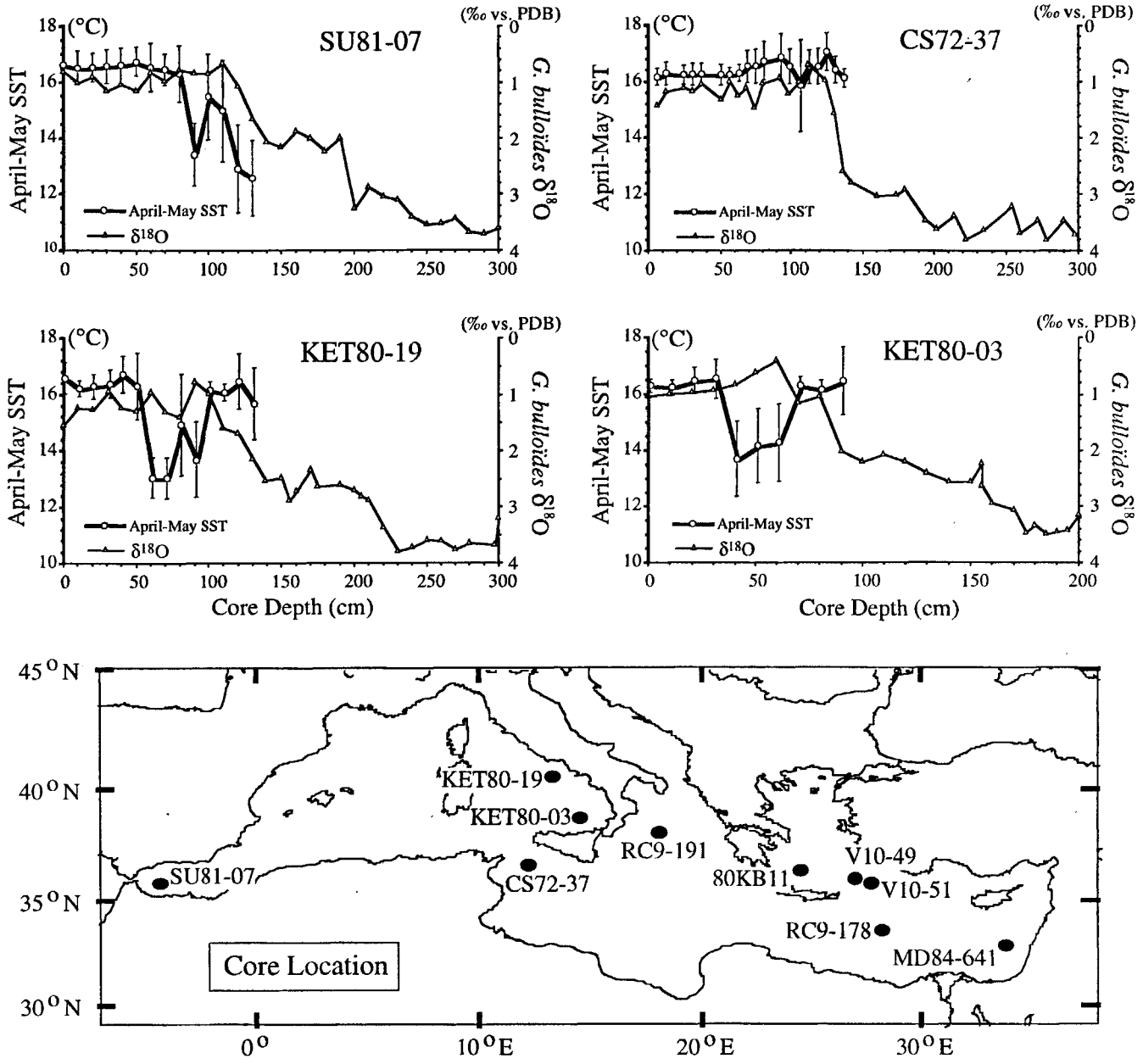

Figure 5*a*

A: Plot of the G. bulloides $\delta^{18}O$ value and April-May SST estimated by the modern analog technique along four Mediterranean cores. A map with core location is also shown.

Surface water $\delta^{18}O$ values were derived for both April-May and October-November when *G. bulloides* and *G. ruber* were present in the same core. The accuracy of the $\delta^{18}O$ estimates depends critically on the accuracy of the SST estimates derived from the transfer function. A 1 °C error in SST value would result in a 0.23°/$_{oo}$ error in the calculated sea water $\delta^{18}O$ value. Adding the 0.07°/$_{oo}$ error associated with the mass spectrometric measurements of foraminiferal $\delta^{18}O$, we conclude that the error in the past sea water $\delta^{18}O$ value is ± 0.30°/$_{oo}$.

The difference between $\delta^{18}O$ estimates derived from *G. bulloides* and *G. ruber* in the same core is lower than 0.22°/$_{oo}$, a value which is in agreement with the theoretical statistical distribution of two estimates known independently with a statistical error of 0.30°/$_{oo}$. Under modern conditions, the amplitude of seasonal surface water $\delta^{18}O$ variations is lower than 0.1°/$_{oo}$ (Table 4). We therefore took the mean value of the April-May and October-November estimates as a best estimate of the sea water $\delta^{18}O$ during the peak of the sapropel event. We neglected possible effects of the hydrological changes on the measured $\delta^{18}O$ values derived from species living at different depths (Williams *et al.*, 1978).

The geographical pattern of sea water $\delta^{18}O$ during S_1 (Fig. 6*a*) was strikingly different from the present. Under modern conditions, salinity and $\delta^{18}O$ increase while surface water flows eastward and northward from Gibraltar Strait, because the freshwater budget of the Mediterranean Sea is

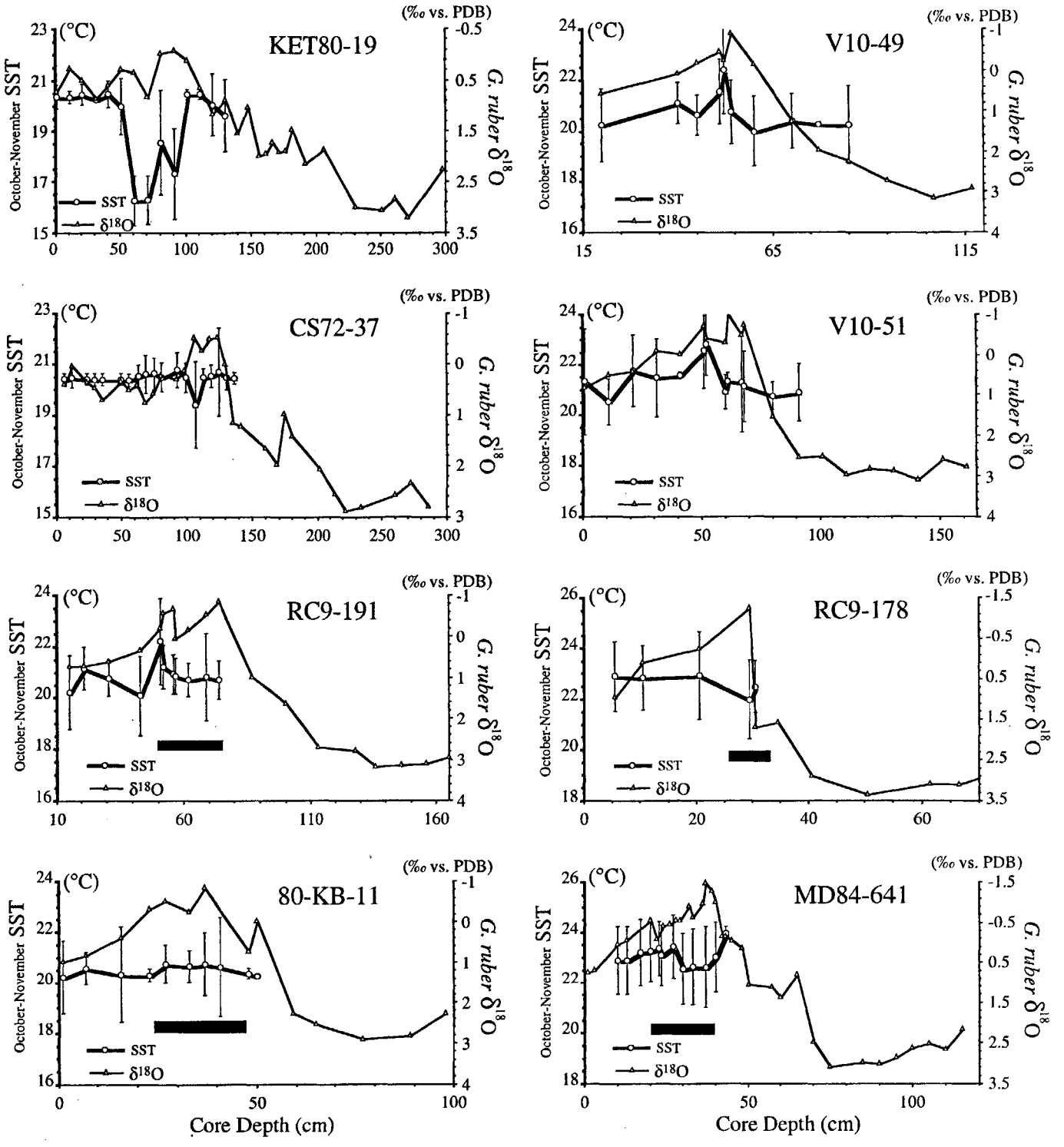

Figure 5*b*

B: Plot of the G. ruber $\delta^{18}O$ composition and October-November SST estimated by the modern analog technique along eight Mediterranean cores. When reliable, sapropel positions are marked by thick black lines.

negative (evaporation exceeds the sum of precipitation and continental runoff). The highest values are found in the easternmost basin, where salinity and $\delta^{18}O$ values exceed those of Gibraltar by 3 and 1.3‰ respectively (Table 4). By contrast, during S_1, no sea surface $\delta^{18}O$ increase is observed in the western basin (Fig. 6*a*). Sea water $\delta^{18}O$ values were approximately constant, while water moved toward the Tyrrhenian Sea and the Siculo-Tunisian Strait. In the eastern basin, $\delta^{18}O$ values exhibit a greater variability and some regional scatter. Low values are found east of the mouth of the Nile river, but also in the Ionian and the Levantine basins, with a mean value only about 0.14‰ higher than that of the western basin.

Sea water $\delta^{18}O$ variations in the past reflect both global changes due to continental ice volume variations and local

Table 4

Data used for the reconstruction of the Mediterranean Sea surface salinity during the last sapropel. Except for the Alboran and Tyrrhenian Seas, where a cooling of 1.5 °C and 2.5 °C respectively, is observed, sapropel SST is taken to be equivalent to the modern one in the eastern Mediterranean basin. Growth temperature of G. bulloides *and* G. ruber *is found to be equivalent to the Mean (April-May) SST and Mean (October-November) SST respectively (see text). The modern sea surface $\delta^{18}O$ was calculated from the Levitus (1982) salinity data using the Mediterranean surface water $\delta^{18}O$/Salinity relationships (Fig. 3). The sapropel sea water $\delta^{18}O$ was calculated by the use of the foraminiferal $\delta^{18}O$ from 47 Mediterranean cores. Sea surface $\delta^{18}O$ anomaly was calculated as the difference between sapropel and modern values.*
Most of the foraminiferal $\delta^{18}O$ values measured at Gif have been published (Fontugne et al., 1989; 1994; Paterne et al., 1986; 1988).

Core	Latitude	Longitude	Foram	Sapropel foram. growth T (°C)	Sapropel foram. $\delta^{18}O$	Sapropel sea surface $\delta^{18}O$/ SMOW	Modern sea surface salinity	Modern sea surface $\delta^{18}O$/ SMOW	Sapropel sea surface $\delta^{18}O$/ anomaly	Sapropel sea surface safinity	Data source
KC82-41	36°00'N	04°24'W	*G. bulloides*	14.95	0.40	0.2	36.59	0.82	−0.6	35.1	1
KS82-30	36°27'N	03°53'W	*G. bulloides*	14.88	0.46	0.3	36.65	0.85	−0.6	35.2	1
SU81-07	35°57'N	03°48'W	*G. bulloides*	15.01	0.66	0.5	36.59	0.82	−0.3	35.8	Gif
KS82-31	36°09'N	03°16'W	*G. bulloides*	14.88	0.47	0.3	36.65	0.85	−0.6	35.3	1
KS82-32	36°07'N	02°07'W	*G. bulloides*	15.47	0.15	0.1	36.74	0.88	−0.8	34.8	1
SU81-03	37°58'N	00°50'E	*G. bulloides*	15.28	0.78	0.7	37.13	1.04	−0.4	36.2	Gif
70KS06	38°31'N	04°00'E	*G. bulloides*	16.63	−0.20	0.0	37.07	1.02	−1.0	34.6	2
KET80-40	36°47'N	11°49'E	*G. bulloides*	16.01	0.76	0.8	37.24	1.09	−0.3	36.6	Gif
CS72-37	36°41'N	12°17'E	*G. ruber*	20.84	−0.54	0.6	37.56	1.22	−0.6	36.1	Gif
CS72-37	36°41'N	12°17'E	*G. bulloides*	16.09	0.70		37.32	1.12	−0.3	36.5	Gif
KET80-19	40°33'N	13°21'E	*G. bulloides*	13.75	0.77	0.3	37.92	1.37	−1.1	35.3	Gif
KET80-19	40°33'N	13°21'E	*G. ruber*	17.71	−0.08	0.4	37.98	1.39	−1.0	35.5	Gif
KET80-04	39°40'N	13°34'E	*G. bulloides*	13.83	0.79	0.3	37.86	1.34	−1.0	35.4	Gif
DED87-07	39°41'N	13°35'E	*G. bulloides*	13.83	0.77	0.3	37.86	1.34	−1.0	35.4	Gif
DED87-07	39°41'N	13°35'E	*G. ruber*	17.86	0.06	0.5	37.93	1.37	−0.8	35.9	Gif
KET80-03	38°49'N	14°30'E	*G. bulloides*	13.92	0.40	0.0	38.09	1.46	−1.5	34.5	Gif
KET80-11	39°10'N	15°05'E	*G. bulloides*	13.70	0.74	0.3	38.14	1.47	−1.2	35.2	Gif
KET82-22	37°56'N	16°53'E	*G. bulloides*	17.04	0.10	0.4	38.21	1.48	−1.1	35.6	Gif
KET82-22	37°56'N	16°53'E	*G. ruber*	20.76	−0.62	0.5	38.25	1.49	−1.0	35.8	Gif
RC9-191	38°11'N	18°02'E	*G. ruber*	20.70	−0.86	0.3	38.48	1.54	−1.3	35.2	Gif
BAN8409GC	34°19'N	20°01'E	*G. ruber*	21.91	−0.70	0.7	38.64	1.57	−0.9	36.3	12
V10-67	35°42'N	20°43'E	*G. ruber*	21.53	−1.20	0.1	38.69	1.58	−1.5	34.8	7
MD84-657	34°03'N	21°31'E	*G. ruber*	21.81	−0.67	0.7	38.73	1.59	−0.9	36.3	Gif
RC9-183	34°30'N	23°25'E	*G. ruber*	21.53	−0.69	0.6	38.91	1.62	−1.0	36.1	Gif
80KB11	36°30'N	24°20'E	*G. ruber*	20.48	−0.86	0.2	38.78	1.60	−1.4	35.1	Gif
82KS04	34°26'N	24°33'E	*G. ruber*	21.53	−1.25	0.1	39.00	1.64	−1.6	34.7	Gif
MD84-656	33°23'N	24°46'E	*G. ruber*	21.95	−1.57	−0.2	38.99	1.64	−1.8	34.2	Gif
67MO-03	34°25'N	24°50'E	*G. ruber*	21.53	−0.60	0.7	39.00	1.64	−0.9	36.3	2
RC9-181	33°25'N	25°00'E	*G. ruber*	22.01	−1.17	0.2	39.06	1.65	−1.4	35.2	8
RC9-180	34°05'N	25°40'E	*G. ruber*	21.54	−0.59	0.7	39.07	1.66	−0.9	36.3	Gif
81-MC-30	34°06'N	25°57'E	*G. ruber*	21.54	−1.26	0.0	39.07	1.66	−1.6	34.7	Gif
TR171-27	33°50'N	25°59'E	*G. ruber*	22.01	−1.10	0.3	39.06	1.65	−1.3	35.3	6
81-MC-28	34°36'N	26°04'E	*G. ruber*	21.62	−1.04	0.3	39.14	1.67	−1.4	35.3	Gif
75-KS52	34°00'N	26°19'E	*G. ruber*	21.62	−0.75	0.6	39.14	1.67	−1.1	36.0	2
V10-49	36°05'N	26°50'E	*G. ruber*	20.14	−0.91	0.1	38.99	1.64	−1.6	34.8	Gif
75-KS50	34°41'N	27°00'E	*G. ruber*	21.81	−0.75	0.6	39.19	1.68	−1.1	36.1	2
V10-58	35°58'N	27°05'E	*G. ruber*	21.16	−0.60	0.6	39.19	1.68	−1.1	36.1	13
82KS-01	34°22'N	27°09'E	*G. ruber*	21.81	−0.48	0.9	39.19	1.68	−0.8	36.7	2
V10-51	35°55'N	27°18'E	*G. ruber*	21.16	−1.02	0.2	39.19	1.68	−1.5	35.1	Gif
RC9-178	33°44'N	27°55'E	*G. ruber*	22.34	−1.25	0.2	39.15	1.67	−1.4	35.1	Gif
P6508-36	32°44'N	30°31'E	*G. ruber*	23.79	−0.88	0.9	39.12	1.66	−0.8	36.8	10
MD84-650	33°40'N	31°45'E	*G. ruber*	23.47	−0.85	0.9	39.19	1.68	−0.8	36.7	Gif
C6-157	33°10'N	32°10'E	*G. ruber*	23.75	−1.00	0.8	39.20	1.68	−0.9	36.5	14
MD90-964	33°03'N	32°39'E	*G. ruber*	23.75	−1.54	0.2	39.20	1.68	−1.4	35.2	Gif
CORE 17	35°30'N	33°20'E	*G. ruber*	23.40	−0.60	1.1	39.25	1.69	−0.6	37.3	11
CORE 190	36°00'N	33°23'E	*G. ruber*	23.40	−0.40	1.3	39.25	1.69	−0.4	37.8	11
MD84-641	33°02'N	33°38'E	*G. ruber*	24.07	−1.49	0.4	39.20	1.68	−1.3	35.5	Gif
MD84-627	32°14'N	33°45'E	*G. ruber*	24.41	−1.39	0.5	39.18	1.68	−1.1	35.9	Gif
GA32	31°57'N	34°21'E	*G. ruber*	24.56	−1.93	0.0	39.16	1.67	−1.7	34.6	15
MD84-629	32°04'N	34°21'E	*G. ruber*	24.56	−1.69	0.3	39.16	1.67	−1.4	35.2	Gif
MD84-632	32°47'N	34°23'E	*G. ruber*	24.56	−1.63	0.3	39.16	1.67	−1.4	35.4	Gif

1- Pujol and Vergnaud-Grazzini, 1989; 2- Vergnaud-Grazzini *et al.*, 1986; 3- Capotondi *et al.*, 1989; 4- Vergnaud-Grazzini *et al.*, 1988; 5- Jorissen *et al.*, 1993; 6- Thunell *et al.*, 1977; 7- Vergnaud-Grazzini, 1975; 8- Vergnaud-Grazzini *et al.*, 1977; 9- Vergnaud-Grazzini *et al.*, 1989; 10- Jenkins and Williams, 1984; 11- Buckley *et al.*, 1982; 12- Cheddadi *et al.*, 1991; 13- Shackleton, unpublished; 14- Luz and Perelis-Grossowics, 1980; 15- Luz, 1979.

A

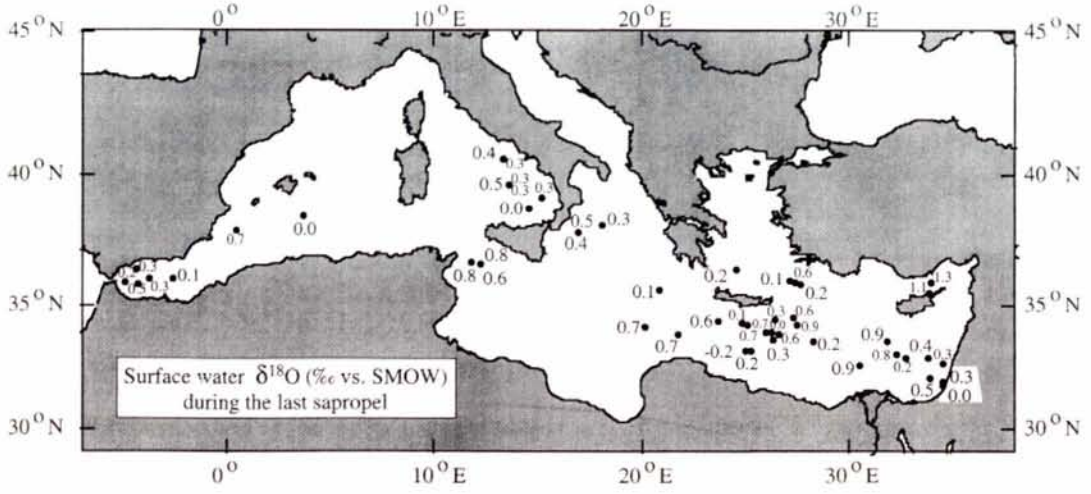

B

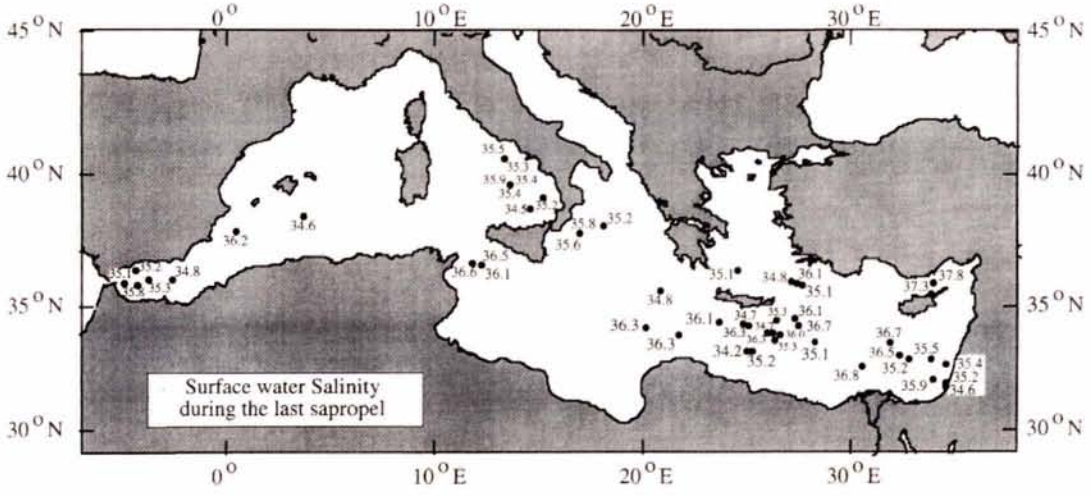

C

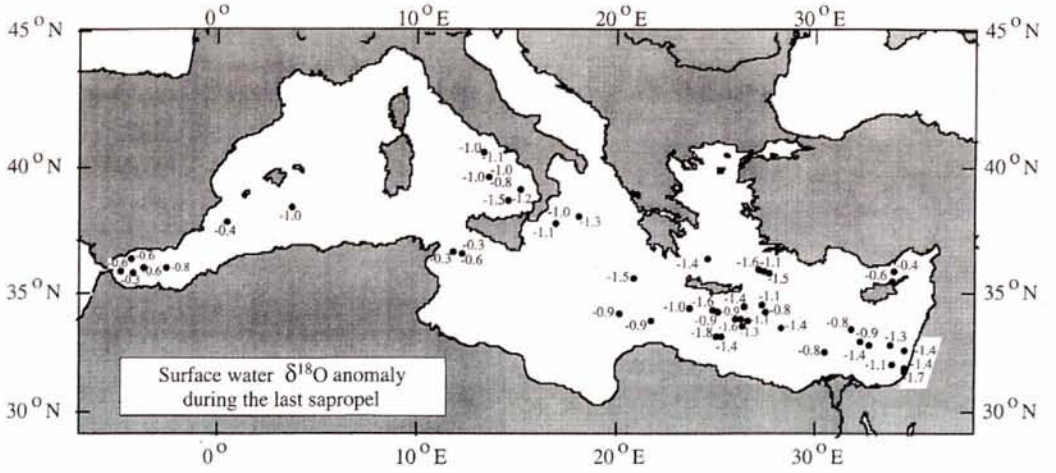

Figure 6

A: Reconstruction of the surface water $\delta^{18}O$ compositions in the Mediterranean Sea during the last sapropel, using foraminiferal $\delta^{18}O$ values from 47 deep-sea cores.
B: Map of the surface water salinity of the Mediterranean Sea during the last sapropel.
C: Map of the surface water $\delta^{18}O$ anomaly (δ_w sapropel – δ_w modern) of the Mediterranean Sea during the last sapropel.

changes in the freshwater budget. At the peak of sapropel S_1, about 8,000 years ago, most continental ice-sheets had already melted (Fairbanks, 1989) and the $\delta^{18}O$ value of the inflowing North Atlantic water was not significantly different from that of today (Duplessy *et al.*, 1993). We therefore estimated the local Mediterranean sea surface $\delta^{18}O$ variations with respect to the modern situation as the difference between the sea water $\delta^{18}O$ during the sapropel and today:

$$\Delta\delta w = \delta^{18}O \text{ sapropel} - \delta^{18}O \text{ modern}$$

Although all the discussions concerning the freshwater budget (precipitation + runoff – evaporation) can be done directly using the estimated $\delta^{18}O$ values, we calculated salinity estimates for surface water, because they are more familiar to oceanographers and they allow to compute density estimates, which are useful to discuss deep water formation during winter. To estimate sea surface salinity, we assumed that the modern sea water $\delta^{18}O$/salinity relationship for the Mediterranean (Fig. 3) was valid during S_1. This is probably an oversimplification. However, as the $\delta^{18}O$ values in the Mediterranean Sea were small, our hypothesis leads us to use that part of the $\delta^{18}O$/salinity relationship which has a slope of 0.41, which is closer to that of the mid-latitude ocean. Using the $\delta^{18}O$/salinity relationship established for the modern Atlantic Ocean (δw = 0.558*Salinity – 19.264; Duplessy *et al.*, 1991) would lead to Mediterranean surface salinity values only slightly lower than those estimated using the previous relationship (Fig. 3). The mean difference between the salinities estimated using these two relations is of about 0.34 ± 0.20, which is within the error on the salinity estimates (≈ 0.73). It should be kept in mind that the error on the SSS estimate is linked to the error on the SST estimate, because, at a given core level, SSS is derived from the comparison of the measured foraminiferal $\delta^{18}O$ value with the faunal SST estimate. At about 15 °C, if SST is underestimated by 1 °C, the salinity will be also underestimated by 0.5, so that the density will be underestimated by only 0.22‰. The reverse is true if SST is overestimated by 1 °C. Taking into account both the 1 °C error estimate on SST and the 0.07‰ error on foraminiferal $\delta^{18}O$ measurements, the total error on density is 0.35‰. Due to the non-linearity of the relationship linking density to SST and SSS, the total error on density is 0.25‰ at 25 °C.

As salinity is linearly linked to sea water $\delta^{18}O$ (Craig and Gordon, 1965), the reconstructed sapropel salinity and sea-water δw maps exhibit similar patterns, with almost homogeneous values over the whole Mediterranean Sea (Fig. 6*a*, *b*). The $\Delta\delta w$ anomaly (Fig. 6*c*) is negative in all Mediterranean basins: the sea surface $\delta^{18}O$ was lower than today by 0.58‰ in the Alboran Sea, 1.1‰ in the Tyrrhenian Sea and more than 1.25‰ in the easternmost Mediterranean Sea. Since the modern west-east $\delta^{18}O$/salinity gradient almost disappeared during S_1, the west to east gradient of $\Delta\delta w$ mirrors the modern situation: the greater the modern evaporation and salinity increase, the higher the anomaly calculated for S_1.

DISCUSSION

During S_1, the planktonic foraminiferal fauna records a 1.5 °C to 2.5 °C cooling in the western Mediterranean basin, while the eastern basin did not exhibit significant SST changes. In the Atlantic Ocean, a cooling of smaller magnitude has been reported at the same time off Portugal (Bard *et al.*, 1989; Duplessy *et al.*, 1992). Simultaneously, vegetation on the continents surrounding the Mediterranean Sea reflects a climate deterioration, although the impact of temperature and moisture changes on the vegetation is difficult to separate. In southern Spain, the Padul pollen sequence exhibits a decrease in arboreal pollen between 9,300 ± 90 years B.P. and 8,200 ± 80 years B.P. (Pons and Reille, 1988). A similar climatic deterioration may also explain the oak pollen decrease at about 8,200 years B.P. in several continental sequences of the Atlantic coast (Watts, 1986). By contrast, the modern vegetation pattern is established between 10,500 and 9,000 years B.P. in mountainous borderlands of Greece and Turkey (Bottema, 1991). Therefore, the West-East dissymmetry of the Mediterranean SST pattern was also reflected in the continental environment.

In the Mediterranean Sea, surface water $\delta^{18}O$ changes result from changes of the local freshwater budget. Meltwater from the European/Asian ice-sheets and huge Nile floods have been abundantly invoked to explain sapropel formation in the eastern basin (Rossignol-Strick *et al.*, 1982; Rossignol-Strick, 1985; Muerdter *et al.*, 1984; Rohling and Hilgen, 1991). Our reconstruction shows that enhanced discharge of the Nile river explains only the salinity drop observed in the easternmost Levantine Sea in agreement with Fontugne *et al.* (1994). Melting of the Eurasian continental ice sheets was almost finished at the time of sapropel S_1 (Grosswald, 1980; Hughes *et al.*, 1981). The similarity of $\delta^{18}O$ values in the Levantine, Ionian and Aegean Seas reflects a source of freshwater uniformly distributed over the whole area, most likely originating from increased precipitation.

Various environmental markers show that pluvial conditions, related to the "Grand Humide" period in the Sahara, prevailed from about 10,000 to 4,000 years B.P. as evidenced by lacustrine deposits, large Nile floods and intensified speleothem growth over the southern and eastern Mediterranean borderlands (Street and Grove, 1979; Adamson *et al.*, 1980; Nicholson and Flohn, 1980; Pachur and Kröpelin, 1987; Goodfriend, 1988; Fontes and Gasse, 1991; Petit-Maire *et al.*, 1991; Callot and Fontugne, 1992; Geyh, 1994). Simultaneously, enhanced wetness over the continent bordering the northern Mediterranean Sea was reflected by high lake levels and high river discharge (Harrison *et al.*, 1991; Starkel, 1991). Therefore increased river runoff from all the Mediterranean borderlands, together with a change of the freshwater budget over the whole Mediterranean area, provide a reasonable explanation for the surface water salinity decrease reconstructed during S_1.

Surface water salinity was maintained at values close to that of the Alboran Sea in the western and eastern basins. This pattern suggests that the freshwater budget

was nearly equilibrated (P + R – E ≈ 0) over the whole Mediterranean Sea. In such a situation, the surface salinity is almost independent of the surface water residence time, which is mainly governed by the rate of water exchange through the Gibraltar Strait. Since the modern net water loss to the atmosphere is about 1000 mm/year, an equivalent yearly increase in the supply of freshwater is necessary to equilibrate the S_1 freshwater budget, if we assume that there was no change in the evaporation rate during the Holocene. The total freshwater input (P + R) into the basin would thus be about three times higher than today (about 560 mm).

Changes in the freshwater budget of the Mediterranean Sea have had a great impact on its circulation. Under present conditions, the combined effects of salinity increase and winter cooling in several basins (Levantine basin, Gulf of Lion) permits the formation of dense intermediate and deep waters. Their high density in the vicinity of Gibraltar ($\sigma \approx 28.67$) is mainly due to their high salinity (≈ 37.9). In the North Atlantic Ocean off the Gibraltar Strait, subsurface waters at the sill level (300 m water depth) have a salinity of 35.75 and a temperature close to 13 °C ($\sigma \approx 27.01$). The Mediterranean water density at the sill level is therefore ≈ 1.65‰ higher than that of the North Atlantic Ocean (Béthoux, 1984). Since the intensity of the water exchange through the Gibraltar Strait depends on the density difference between both sides, the modern steep horizontal density gradient allows a strong outflow of the Mediterranean intermediate water toward the North Atlantic and permits pumping and renewal of the deep Mediterranean water (Béthoux, 1984).

During S_1, no current reversal occurred at Gibraltar (Zahn and Sarnthein, 1987; Vergnaud-Grazzini *et al.*, 1989). As the Mediterranean Sea was not a concentration basin, the density gradient could only have been maintained by winter cooling of the western Mediterranean surface water, resulting in the formation of intermediate water cooler than today. In order to maintain the modern East-West negative density gradient at Gibraltar Strait, we calculated that the intermediate water temperature must have been lower or equal to 11.25 °C (Fig. 7) in the western Mediterranean Sea, considering the mean surficial salinity being close to 35.31 and assuming no density change in the North Atlantic Ocean. Assuming that the 2.5 °C surface water cooling was totally transferred to intermediate water, the temperature of western Mediterranean intermediate water would be close to 10.5 °C during S_1, resulting in a density $\sigma = 27.15$. The density difference at the Gibraltar sill depth between the western Mediterranean Sea and the North Atlantic Ocean ($\sigma = 27{,}01$) was therefore drastically reduced during S_1 (about 0.14). Using the relationship established by Béthoux (1984) to estimate the flux of water exchanged through the Gibraltar Strait, we calculated that the Mediterranean outflow was only 14% of the modern flux, assuming that the sill geometry did not change over the past 8,000 years. As a consequence, the residence time of Mediterranean deep water increased strongly at the time of sapropel S_1.

Eastern intermediate water forms today during winter in the southeastern Aegean Sea and close to Rhodes and northwestern Cyprus. This area is documented by three

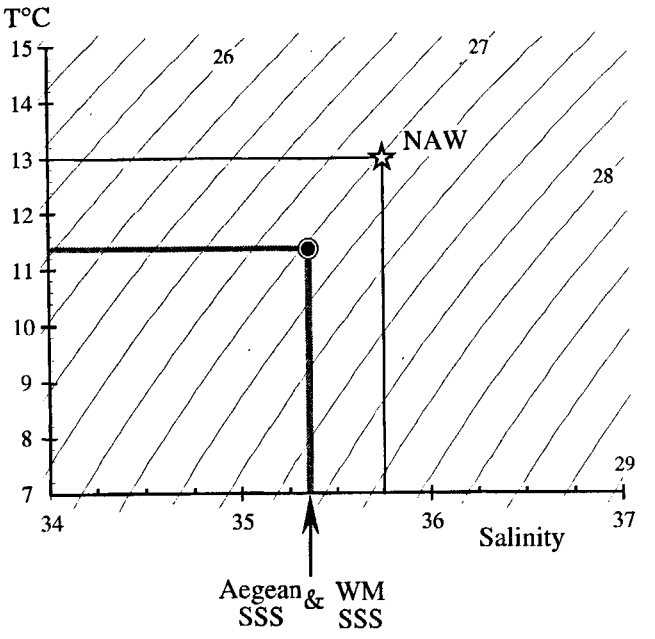

Figure 7

Temperature/salinity/density diagram. NAW = Levitus T/S of the North Atlantic water off Gibraltar Strait at the sill level (300 m); WM SSS and Aegean SSS = mean sea surface salinity of the western Mediterranean Sea and of the south-eastern Aegean basin respectively, at the time of the last sapropel.

cores V10-49, V10-51 and V10-58. Taking into account the mean salinity estimate of 35.33 during S1 and the density of the western intermediate water, a temperature of about 10.5 °C would be required to ensure a density sufficiently high to permit intermediate water crossing the Siculo-Tunisian Strait (Fig. 7). In order to get such a low temperature, intermediate water should have been cooler than today by 4.5 °C. Such a cooling is not realistic because SST estimates during S_1 are approximately similar to modern values. Therefore surface waters were too warm to allow formation of intermediate water in the Levantine basin. As the SSTs of the eastern basin are higher than those of the western basin and as similar salinity values are found on both sides of the Siculo-Tunisian Strait, the surface water density was higher in the western basin than in the eastern Sea. Such a pattern would trigger a reversal of the water flow at the strait, *i.e.* an eastward deep water inflow compensated by a westward surficial flow. Such a circulation reversal, already suggested by Thunell and Williams (1989), resulted in the water column stratification in the eastern basin and the development of permanent pycnocline separating warm surface water from cooler intermediate and deep waters originating from the western Mediterranean Sea. This hydrological structure was responsible for the inhibition of direct deep supply of dissolved oxygen and for the development of anoxic conditions permitting the preservation of organic matter on the bottom in the eastern Sea.

CONCLUSION

During the last sapropel event, SSTs in the Mediterranean Sea were similar to those of today in the eastern basin, but

cooler by about 1.5 to 2.5 °C in the western basin. This SST contrast between the western and eastern Mediterranean basins is consistent with the observed vegetational changes on the continental borderlands.

Sea surface salinity was everywhere lower than today during sapropel S_1, and almost homogeneous over the whole Mediterranean Sea. The Mediterranean region had thus experienced marked pluvial conditions, so that the freshwater budget was nearly equilibrated. This rainfall spike coincides with the peak of the humid period described in the Sahara, but also with conditions wetter than today over most of Europe. The sapropel event was associated with a peculiar hydrological situation, as the Mediterranean Sea ceased to be a concentration basin. Despite the strong sea surface salinity decrease, formation of Mediterranean intermediate waters was maintained, although drastically reduced, during S_1 in the western basin as a consequence of the SST decrease, but ceased in the whole eastern basin which was not affected by SST changes.

Acknowledgements

We thank D. Dole, E. Kaltnecker, H. Leclaire, B. Le Coat, J. Tessier and N. Tisnerat for their help in the isotopic analyses, and A. Juillet-Leclerc, E. Michel, M. Montacer for useful discussions. This work was supported by CNRS, CEA, INSU (PNEDC), TAAF and MAST CLIVAMP project n° MAS3-CT95-0043. N. Kallel gratefully acknowledges the support of the Ministère Français des Affaires Etrangères and Tunisian DGRST (projet CMCU n° 97/F1002).

REFERENCES

Adamson D.A., F. Gasse, A. Street, A.J. Williams (1980). Late Quaternary history of the Nile. *Nature* **288**, 50-55.

Bard E., R. Fairbanks, M. Arnold, P. Maurice, J. Duprat, J. Moyes, J.-C. Duplessy (1989). Sea-level estimates during the last deglaciation based on $\delta^{18}O$ and accelerator mass spectrometry ^{14}C ages measured in *Globigerina bulloides*. *Quat. Res.* **31**, 381-391.

Bé A., W.H. Berger, D.S. Tolderlund (1971). Distribution and ecology of living planktonic foraminifera in surface waters of the Atlantic and Indian oceans. *In:* (B.M. Funnell, W.R. Riedel, Eds.), *The Micropaleontology of the Oceans*, 105-149, Cambridge University Press.

Béthoux J.P. (1984). Paléo-hydrologie de la Méditerranée au cours des derniers 20 000 ans. *Oceanologica Acta* **7**, 43-48.

Berger W.H. (1976). Biogenic deep-sea sediments: production preservation and interpretation. *In: "Chemical Oceanography"*. Ed. by J.P. Riley and R. Chester, Academic, San Diego, Calif., 265-388.

Bottema S. (1991). Pollen proxy data from southeastern Europe and the Near East. *In: "Evaluation of climate proxy data in relation to the Eurpean Holocene"*. Ed. by B. Frenzel, Stuttgart; Jena; New York: G. Fisher, 63-79.

Bradley W.H. (1938). Mediterranean sediments and Pleistocene sea levels. *Science* **88**, 376-379.

Buckley H.A., L.R. Johnson, N.J. Shackleton, R.A. Blow (1982). Late glacial to recent cores from the Eastern Mediterranean. *Deep-Sea Res.* **35**, 739-766.

Callot Y., M. Fontugne (1992). Les étagements de nappes dans les paléolacs holocènes du nord-est du Grand Erg Occidental (Algérie). *C.R. Acad. Sci. Paris* **315**, 471-477.

Calvert S.E. (1983). Geochemistry of Pleistocene sapropels and associated sediments from the Eastern Mediterranean. *Oceanologica Acta* **6**, 255-267

Calvert S.E., B. Nielsen, M.R. Fontugne (1992). Evidence from nitrogen isotope ratios for enhanced productivity during formation of Eastern Mediterranean sapropels. *Nature* **359**, 223-225.

Capotondi L., A.M. Borsetti, C. Vergnaud-Grazzini, S. D'Onofrio (1989). Biostratigrafia e stratigrafia isotopica della corota AC 85-4: considerazioni sulla paleoceanografia tardo-quaternaria del Mar Tirreno orientale. *Giornale di Geologia*, ser. 3, 519, 201-212.

Cheddadi R., M. Rossignol-Strick, M. Fontugne (1991). Eastern Mediterranean paleoclimates from 26 to 5 ka B.P. documented by pollen and isotopic analysis of a core in the anoxic Bannock Basin. *Mar. Geol.* **100**, 53-66.

Cita M.B., C. Vergnaud-Grazzini, C. Robert, H. Chamley, N. Ciaranfi, S. Donofrio (1977). Paleoclimatic record of a long deep-sea core from the Eastern Mediterranean. *Quat. Res.* **8**, 205-235.

Craig H., A. Gordon (1965). Deuterium and oxygen 18 variations in the ocean and the marine atmosphere. *In: "Stable isotopes in Oceanic Studies and Paleotemperatures". Spoleto*, E. Tongiorgi, ed. CNR Pisa, 9-130.

Duplessy J.-C. (1972). La géochimie des isotopes stables du carbone dans la mer. *Thesis, Université de Paris, France*, 196 p.

Duplessy J.-C., M. Fieux (1972). Etude isotopique des apports d'eau douce en Méditerranée occidentale. *Rapp. Comm. int. Mer Médit.* **21**, 197-201.

Duplessy J.-C., L.D. Labeyrie, A. Juillet-Leclerc, F. Maître, J. Duprat, M. Sarnthein (1991). Surface salinity reconstruction of the North Atlantic ocean during the last glacial maximum. *Oceanologica Acta* **14**, 311-324.

Duplessy J.-C., L.D. Labeyrie, M. Arnold, M. Paterne, J. Duprat, T.C.E. van Weering (1992). Changes in surface salinity of the North Atlantic ocean during the last deglaciation. *Nature* **358**, 485-487.

Duplessy J.-C., E. Bard, L.D. Labeyrie, J. Duprat, J. Moyes (1993). Oxygen isotope records and salinity changes in the Northeastern Atlantic Ocean during the Last 18 000 years. *Paleoceanography* **8**, 341-350.

Epstein S., R. Buchsbaum, H.A. Lowenstam, H.C. Urey (1953). Revised carbonate-water isotopic temperature scale. *Geol. Soc. Am. Bull.* **64**, 1315-1325.

Fairbanks R.G. (1989). A 17 000-year glacio-eustatic sea level record: influence of glacial melting rates on the Younger Dryas event and deep ocean circulation. *Nature* **342**, 637-642.

Fontes J.C., F. Gasse (1991). "Palaeohydrology in Africa" program: objectives, methods, major results. *Palaeogeogr., Palaeoclim., Palaeoecol.* **84**, 191-215.

Fontugne M., M. Paterne, S.E. Calvert, A. Murat, F. Guichard, M. Arnold (1989). Adriatic deep water formation during the Holocene: implication for the reoxygenation of the deep Eastern Mediterranean sea. *Paleoceanography* **4**, 199-206.

Fontugne M., M. Arnold, L. Labeyrie, M. Paterne, S.E. Calvert, J.-C. Duplessy (1994). Palaeoenvironment, Sapropel chronology and Nile river discharge during the last 20 000 years as indicated by deep sea sediment records in the Eastern Mediterranean. *In: "Late Quaternary chronology and paleoclimates of the Eastern*

Mediterranean". Ed. by O. Bar-Yosef and R.S. Kra, Radiocarbon: 75-88.

Geyh M.A. (1994). The paleohydrology of the eastern Mediterranean. *In: "Late Quaternary Chronology and paleoclimates of the Eastern Mediterranean".* Ed. by O. Bar-Yosef and R.S. Kra. Radiocarbon, 131-145.

Goodfriend G.A. (1988). Mid Holocene rainfall in the Negev Desert from ^{13}C of land snail shell organic matter. *Nature* **333**, 757-760.

Grosswald M.G. (1980). Late Weichselian ice sheet of Northern Eurasia. *Quat. Res.* **13**, 1-32.

Harrison S.P., I.C. Prentice, P.J. Bartlein (1991). What climate models can tell us about the Holocene palaeoclimates of Europe. *In: "Evaluation of climate proxy data in relation to the European Holocene".* Ed. by B. Frenzel, Stuttgart; Jena; New York: G. Fisher, 285-299.

Howell M.W., R.C. Thunell (1992). Organic carbon accumulation in Bannock basin: Evaluating the role of productivity in the formation of eastern Mediterranean sapropels. *Mar. Geol.* **103**, 461-471.

Huang T.C., D.G. Stanley (1972). Western Alboran sea: sediment dispersal, pounding and reversal of currents. *In: "The Mediterranean sea".* Ed. by D.G. Stanley, Dowden, Hutchinson and Ross, Stroudsburg, Pa., 631-643.

Hughes T.J., G.H. Denton, B.G. Andersen, D.H. Schilling, J.L. Fastook, C.S. Lingle (1981). The last great ice sheets: a global view. *In: The last great ice sheets.* Eds. Denton, G.H. and T.J. Hughes, J. Wiley and Sons, 275-317.

Hutson W.H. (1979). The Aghulas current during the late Pleistocene: analysis of modern analogs. *Science* **207**, 227-238.

Jenkins J.A., D.F. Williams 1984. Nile water as a cause of Eastern Mediterranean sapropel formation: evidence for and against. *Mar. Micropal.* **9**, 521-534.

Jorissen F.J., A. Asioli, A.M. Borsetti, L. Capotondi, J.P. de Visser, F.J. Hilgen, E.J. Rohling, K. van der Borg, C. Vergnaud-Grazzini, W.J. Zachariasse (1993). Late Quaternary central Mediterranean biochronology. *Mar. Micropal.* **21**, 169-189.

Levitus S. (1982). Climatological atlas of the world ocean. NOAA Professional Paper n°13, Rockville, Maryland, USA.

Luz B. (1979). Paleo-oceanography of the post glacial Eastern Mediterranean. *Nature* **278**, 847-848.

Luz B., L. Perelis-Grossowicz (1980). Oxygen isotopes, biostratigraphy and recent sedimentation rates in the Eastern Mediterranean off Israel. *Israel J. Earth Sci.* **29**, 140-146.

Muerdter D.R., J.P. Kennett, R.C. Thunell (1984). Late Quaternary sapropel sediments in the Eastern Mediterranean Sea: faunal variations and chronology. *Quat. Res.* **21**, 385-403.

Nicholson S.E., H. Flohn (1980). African environmental and climatic changes and the general atmospheric circulation in late Pleistocene and Holocene. *Climatic Change* **2**, 313-348.

Overpeck J.T., T. Webb III, I.C. Prentice (1985). Quantitative interpretation of fossil pollen spectra: dissimilarity coefficients and the method of modern analogs. *Quat. Res.* **23**, 87-108.

Pachur H.J., S. Kröpelin (1987). Wadi Howar: paleoclimatic evidence from an extinct river system in the Southeastern Sahara. *Science* **237**, 289-300.

Paterne M., F. Guichard, J. Labeyrie, P.Y. Gillot, J.-C. Duplessy (1986). Tyrrhenian Sea tephrachronology of the oxygen isotope record for the past 60 000 years. *Mar. Geol.* **72**, 259-285.

Paterne M., F. Guichard, J. Labeyrie (1988). Explosive Activity of the South Italien volcanoes during the past 80 000 years as determined by marine tephrochronology. *J. Volcanol. Geotherm. Res.* **34**, 153-172.

Petit-Maire N., P.F. Burollet, J.L. Ballais, M. Fontugne, J.C. Rosso, A. Lazaar (1991). Paléoclimats holocènes du Sahara septentrional. Dépôts lacustres et terrasses alluviales en bordure du Grand Erg Oriental à l'extrême-sud de la Tunisie. *C R. Acad. Sci. Paris* **312**, 1661-1666.

Pierre C (1997). The oxygen and carbon isotope distribution in the Mediterranean water masses, *Marine Geology*, in press.

Pierre C., C. Vergnaud-Grazzini, D. Thouron, J.-F. Saliège (1986). Compositions isotopiques de l'oxygène et du carbone des masses d'eau en Méditerranée. *Mem. Soc. Geol. It.* **36**, 165-174.

Pierre C., A. Vangriesheim, E. Laube-Lenfant (1994). Variability of water masses and of organic production - regeneration systems as related to eutrophic, mesotrophic and oligotrophic conditions in the northeast Atlantic Ocean, *J. Mar. Systems* **5**, 159-170.

Pons A., M. Reille (1988). The Holocene and upper Pleistocene pollen record from Padul (Granada, Spain): A new study. *Palaeogeogr., Palaeoclim., Palaeoecol.* **66**, 243-263

Prell W. (1985). The stability of low-latitudes sea surface temperatures: an evaluation of the CLIMAP reconstruction with emphasis on the positive SST anomalies. p. 60. Technical Report. TR025, United States Department of Energy, Washington, DC.

Pujol C., C. Vergnaud-Grazzini (1989). Palaeoceanography of the last deglaciation in the Alboran sea (Western Mediterranean). Stable isotopes and planktonic foraminiferal records. *Mar. Micropal.* **15**, 153-179.

Pujol, C., C. Vergnaud-Grazzini (1995). Distribution patterns of live planktic foraminifers as related to regional hydrography and productive systems of the Mediterranean Sea. *Mar. Micropal.* **25**, 187-217.

Rohling E.J. (1991). Shoaling of the Eastern Mediterranean pycnocline due to reduction of excess evaporation: implications for sapropel formation. *Paleoceanography* **6**, 747-753.

Rohling E.J. (1994). Review and new aspects concerning the formation of eastern Mediterranean sapropels. *Mar. Geol.* **122**, 1-28.

Rohling E.J., W.W.C. Gieskes (1989). Late Quaternary changes in Mediterranean intermediate water density and formation rate. *Paleoceanography* **4**, 531-545.

Rohling E.J., F.J. Hilgen (1991). The eastern Mediterranean climate at times of sapropel formation: a review. *Geol. in Minjbouw* **70**, 253-264.

Rossignol-Strick M., W. Nesteroff, P. Olive, C. Vergnaud-Grazzini (1982) After the Deluge: Mediterranean stagnation and sapropel formation. *Nature* **295**, 105-110.

Rossignol-Strick M. (1985). Mediterranean quaternary sapropels, an immediate response to the African monsoon to variation of insolation. *Palaeogeogr., Palaeoclim., Palaeoecol.* **49**, 237-263.

Ryan W.B.F., M.B. Cita (1977). Ignorance concerning episodes of ocean-wide stagnation. *Mar. Geol.* **23**, 193-215.

Sarmiento J., T. Herbert, J. Toggweiler (1988). Mediterranean nutrient balance and episodes of anoxia. *Global Biogeochem. Cycles* **2**, 427-444.

Schrader H., A. Matherne (1981). Sapropel formation in the Eastern Mediterranean sea: evidence from preserved opal assemblages. *Micropaleontology* **27**, 191-203.

Shackleton N.J. (1974). Attainment of isotopic equilibrium between ocean water and the benthonic foraminifera genus Uvigerina: isotopic changes in the ocean during the last glacial. Colloque CNRS n°219, Centre National de la Recherche Scientifique, Paris: 203-210.

Stahl W., U. Rinow (1973). Sauerstoffisotopenanalysen an Mittelmeerwasser, ein Beitrag zur Problematik von Palaotemperatur Bestimmungen. *Meteor Forschungsergeb. Reihe C.* **14**, 55-59.

Starkel L. (1991). Fluvial environments as a source of information on climatic changes and human impact in Europe. *In: "Evaluation of climate proxy data in relation to the European Holocene".* Ed. by B. Frenzel, Stuttgart; Jena; New York: G. Fisher, 241-254.

Street F.A., A.T. Grove (1979). Global maps of lake-level fluctuations since 30 000 yr. B.P. *Quat. Res.* **12**, 83-118.

Sutherland H., S.E. Calvert, R.J. Morris (1984). Geochemical studies of the recent sapropel and associated sediment from Hellenic outer Ridge, Eastern Mediterranean sea. Mineralogy and chemical composition, *Mar. Geol.* **56**, 79-92.

Thiede J. (1978). A glacial Mediterranean. *Nature* **276**, 680-683.

Thunell R.C. (1979). Eastern Mediterranean sea during the last glacial maximum: a 18 000 years B.P. reconstruction. *Quat. Res.* **11**, 353-372.

Thunell R.C., D.F. Williams, J.P. Kennett (1977). Late Quaternary paleoclimatology, stratigraphy and sapropel history in Eastern Mediterranean deep sea-sediments. *Mar. Micropal.* **2**, 371-388.

Thunell R.C., D.F. Williams (1989). Glacial-Holocene salinity changes in the Mediterranean sea: hydrographic and depositional effects. *Nature* **338**, 493-496.

Thunell R.C., D.F. Williams, P.R. Belyea (1984). Anoxic events in the Mediterranean sea in relation to the evolution of late Neogene climates. *Mar. Geol.* **59**, 105-134.

Thunell R.C., D.F. Williams, M. Howell (1987). Atlantic-Mediterranean water exchange during the late Neogene. *Paleoceanography* **2**, 661-678.

Troelstra S.R., G.M. Ganssen, K. van der Borg, A.F.M. de Jong (1991). A late Quaternary stratigraphic framework for Eastern Mediterranean sapropel S_1 based on AMS ^{14}C dates and stable oxygen isotopes. *Radiocarbon* **33**, 15-21.

Vergnaud-Grazzini C. (1975). $\delta^{18}O$ changes in foraminifera carbonates during the last 10^5 years in the Mediterranean sea. *Science* **190**, 272-274.

Vergnaud-Grazzini C., W.B.F Ryan, M.B. Cita (1977). Stable isotope fractionation, climate change and episodic stagnation in the Eastern Mediterranean during the Late Quaternary. *Mar. Micropal.* **2**, 353-370.

Vergnaud-Grazzini C., M. Devaux, J. Znaidi (1986). Stable isotope "anomalies" in the Mediterranean Pleistocene records. *Mar. Micropal.* **10**, 35-69.

Vergnaud-Grazzini C., A.M. Borsetti, F. Cati, P. Colantoni, S. D'Onofrio, J.F. Saliège, R. Sartori, R. Tampieri (1988). Palaeoceanographic record of the last deglaciation in the strait of Sicily. *Mar. Micropal.* **13**, 1-21.

Vergnaud-Grazzini C., M. Caralp, J.-C. Faugères, E. Gonthier, F. Grousset, C. Pujol, J.F. Saliège (1989). Mediterranean outflow through the Strait of Gibraltar since 18 000 years B.P. *Oceanologica Acta* **12**, 305-324.

Watts W.A. (1986). Stages of climatic change from full Glacial to Holocene in Northwest spain, Southern France and Italy: a comparison of the Atlantic coast and the Mediterranean basin. *In: "Current issues in climate research".* Ed. by A. Ghazi, R. Fantechi, Proc. EC Climatology Programme Symposium, Sophia-Antipolis, France, 101-112.

Williams D.F., R.C. Thunell, J.P. Kennett (1978). Periodic freshwater flooding and stagnation of the Eastern Mediterranean Sea during the Late Quaternary. *Science* **201**, 252-254.

Zahn R., M. Sarnthein (1987). Benthic isotope evidence for changes of the Mediterranean outflow during the late Quaternary. *Paleoceanography* **2**, 543-559.